 MCB, vol.15, no.3, pp.155-176, 2018

A Coupled Friction-Poroelasticity Model of Chimneying Shows that Confined Cells Can Mechanically Migrate Without Adhesions

Solenne Mondésert-Deveraux[1,*], Rachele Allena[2] and Denis Aubry[1]

Abstract: Cell migration is the cornerstone of many biological phenomena such as cancer metastasis, immune response or organogenesis. Adhesion-based motility is the most renown and examined motility mode, but in an adhesion-free confined environment or simply to achieve a higher migration speed, cells can adopt a very interesting bleb-based migration mode called "chimneying". This mode rests on the sharp synchronization between the active contraction of the cells uropod and the passive friction force between the cell and the confining surface. In this paper, we propose a one dimensional poroelastic model of chimneying which considers the active strains of the cell, but, as an improvement with respect to our previous works, the synchronization between such strains and the friction forces developed by the cell and necessary to move forward is self-determined. The present work allows to deepen our knowledge on chimneying which is still poorly understood from a mechanical point of view. Furthermore, our results emphasize the key role of poroelasticity in bleb formation and give new insights on the location and the time-synchronization of the friction force. Further development of this exploratory work could provide a major tool to test hypotheses beforehand and thus focus future experiments on mechanically relevant ones.

Keywords: Poroelasticity, cell migration, chimneying, bleb, finite element.

1 Introduction

Cells can adapt their motility strategy. Cell motility is a fundamental mechanism involved in several biological phenomena such as bone remodelling, immune response and tumorogenesis. Different modes of motility exist, such as flagellar motility [Silflow and Lefebvre (2001)], gliding [Kappe, Buscaglia, Bergman et al. (2004)], swarm-ing [Henrichsen (1972)], mesenchymal [Chhabra and Higgs (2007); Van Haastert (2011)] or amoeboid motility [Charras and Paluch (2008)]. Some cells are able to switch from mesenchymal (F-actin driven pseudopods) to amoeboid (myosin-driven blebs) migration as a reaction to various environments, such as an increased confinement [Ibo, Srivastava, Robinson et al. (2016)]. Mesenchymal motility is based on a tight synchronization between the protrusion-contraction movement of the cell and the adhesion forces exerted by the cell on the substrate and necessary to anchor and move forward. In three-dimensional (3D) confined environments and in the absence of adhesion/traction forces, some cells such as cancer cells are able to adopt an amoeboid mode of invasion forming bleb-like constric-

[1] CentraleSupelec, Laboratoire MSSM at UMR CNRS 8579, 8-10 rue Joliot-Curie, 91190 Gif-sur-Yvette-France.

[2] Arts et Metiers ParisTech, LBM/Institut de Biomécanique Humaine Georges Charpak, 151 bd de l'Hôpital 75013 Paris-France.

* Corresponding Author: Solenne Mondésert-Deveraux. Email: solenne.mondesert@centralesupelec.fr.

tion rings (i.e. membrane protrusions without cytoskeletal elements such as actin filaments) [Wolf, Mazo, Leung et al. (2003); Liu, Le Berre, Lautenschlaeger et al. (2015)] and bypassing the requirement for ExtraCellular Matrix (ECM) degradation [Sahai and Marshall (2003); Friedl (2004)], as it occurs during mes-enchymal migration. In this specific case, the cell migrates through a traction-independent mechanism named "chimneying" because of its resemblance with a technique used by alpinists to climb up rock clefts [Paluch and Raz (2013)]. In fact, the cell generates push-ing forces perpendicular to its membrane [Malawista, de Boisfleury Chevance and Boxer (2000); Lämmermann, Bader, Monkley et al. (2008)] and the result-ing friction is sufficient to ensure the forward movement and may be enhanced by blebbing into gaps and pores within the ECM. This last migration mode is the main focus of this paper.

The importance of interstitial fluid flow in cells. The specificity of bleb-based chimneying migration lies in the ability of the cell to move without the formation of adhesions between the cell and its surrounding and in the absence of actin polymerization. Without two key features of classical mesenchymal migration, one may wonder: What is the motor of such migration mechanism? Some migration modes have been found to be driven by intra-cellular pressure instabilities [Petrie, Koo and Yamada (2014)], or fluid exchanges between the cell and its environment [Stroka, Jiang, Chen et al. (2014)], thus pointing out the importance to take intra-cellular fluid flow into account when dealing with cell mechanics. In fact, the pressure instabilities and the resulting interstitial fluid flow are what drives the formation of a bleb [Maugis, Brugués, Nassoy et al. (2010)].

Bleb-based chimneying migration. Bleb-based migration takes its source in the poroelastic properties of the cytoplasm [Zhou, Martinez and Fredberg (2013); Arroyo and Trepat (2017)]. The life cycle of a bleb can fall into three steps: initiation, growth and retraction [Charras and Paluch (2008)]. An increase in the intra-cellular hydrostatic pressure, coupled with a local weakening of the actin cortex underlying the membrane, can lead to the initiation and the growth of a bleb, while the repairing of the actin cortex forces the bleb to retract. Chimneying is much less studied and described in the literature than mesenchymal migration. Hence, many hypotheses are made but not yet confirmed on the translocation process. In this type of migration strategy, some experimental works have shown a sharp decrease, or a complete lack, of integrin-mediated adhesions [Lämmermann, Bader, Monkley et al. (2008)]. If the cell does not adhere to the substrate, it should oscillate around a stable position, unless another force enables it to move forward. One strong hypothesis is that the cell "pushes" against the confining surface, which gen-erates sufficient friction for it to "stick" to the wall [Hawkins, Piel, Faure-Andre et al. (2009)]. Then, a fine synchronization between the "stick-slip" phases and the life cycle of the bleb is necessary for the cell to have a net forward motion.

Poroelastic models in biology. Cell modeling is not the first field of biomechanics getting into poroelasticity. Such models have been used to model soft tissues [Pena, Bolton and Pickard (1998)], bone [Cowin (1999)], blood vessels [Thiriet (2007)], ECM [Vuong, Rauch and Wall (2017)], cell nucleus [Cao, Moeendarbary, Isermann et al. (2016)] as well as cell cytoplasm [Taber, Shi, Yang et al. (2011); Strychalski, Copos, Lewis et al. (2015); Ghosh, Ozcelikkale, Dutton et al. (2016)]. The cell cytoplasm is often modeled as a viscoelastic medium [Karcher, Lammerding, Huang et al. (2003); Deveraux, Allena and Aubry

(2017)], but the relevance of interstitial fluid flow makes us question this assumption and a poroelastic representation appears as more suited for bleb-based chimneying. Indeed, cell rheology is often explained through viscosity while the poroelasticity theory appears to be more fitted [Moeendarbary, Valon, Fritzsche et al. (2013); Wei, Lan, Liu et al. (2016)]. Among the previously cited poroe-lastic cell models, Strychalski et al. tackled the issue of cell blebbing and cell crawling [Strychalski, Copos, Lewis et al. (2015)] and Taber et al. [Taber, Shi, Yang et al. (2011)] presented a very interesting model of confined actin-polymerization-based migra-tion. Some models for cell blebbing exist without considering poroelasticity [Lim, Koon and Chiam (2013); Woolley, Gaffney and Goriely (2017)], but bleb-based chimneying in-cluding poroelasticity has not yet been studied.

The proposed model. The challenge in bleb-based chimneying is to capture the very fine synchronization between the friction force with the confining surface and the bleb cycle. In this respect, the present paper proposes a one-dimensional (1D) Finite Elements (FE) model of a poroelastic cell. The model revolves around three main ingredients: the constitutive relationship of the material, the active strain-as developed in previous models [Deveraux, Allena and Aubry (2017); Aubry, Thiam, Piel et al. (2014); Allena and Aubry (2012b); Allena (2013); Allena and Aubry (2012a); Allena (2014); Allena, Aubry and Sharpe (2013)]-solely at the rear of the cell and the Coulomb's friction force between the cell and the confining surface. Our goal is to explore a rarely studied motility mode and to show that, in terms of cell-environment interaction, the laws of mechanics alone are surprinsingly sufficient to enable a net forward motion in a non-adhesive migration. Hence, we chose not to model one specific cell phenotype but to develop a generic model that could later on be further enriched to fit a specific cellular type.

2 The poroelastic model

We first write all the equations of the model in 2D in order to stay close to our previously developed models, and will proceed to the 1D reduction on the final equations only.

2.1 Global equations of the model

The cell cytoplasm can be considered as a porous material-made of the cytoskeleton, as well as all the organelles present there-infiltrated with interstitial fluid. In such a configuration, two sorts of fluid-solid interactions may occur. First, a fluid-to-solid interaction takes place when a fluid displacement or an evolution of the intra-cellular pressure induce a variation of the cytoplasm volume. Second, a solid-to-fluid interaction may occur when the mechanical stresses applied to the cell provoke an evolution of the intra-cellular pressure and a displacement of the fluid. Our poroelastic approach is based on the theory developed by Terzaghi in 1936 for geomechanics [Terzaghi (1936)], and taken one step further, for numerical purposes, by Zienkiewicz [Zienkiewicz (1999)]. We consider that the total stress in the material is the superposition of the effective stress and the stress due to the fluid pressure. The effective stress is the Cauchy stress in the dry solid, which then follows the typical stress-strain relationship. As for the pressure, if we freeze the system at a certain time and measure the pressure inside the fluid, the difference between the total stress and the effective stress is the stress exerted by the fluid pressure on the system. In this framework, the total Cauchy stress $\boldsymbol{\sigma}$ is defined as:

$$\boldsymbol{\sigma} = \boldsymbol{\sigma'} - p_f \mathbf{I} \tag{1}$$

where $\boldsymbol{\sigma'}$ is the effective stress in the solid part, p_f is the hydrostatic fluid pressure, and $\mathbf{I}$ is the identity matrix. Biot models usually found in the literature [Taber, Shi, Yang et al. (2011); Strychalski, Copos, Lewis et al. (2015)] offer refined considerations, but the approach in Eq. 1 is accurate enough for our purpose.

The motor of cell blebbing lies in the high contractility of the cell rear, the uropod [Lorentzen, Bamber, Sadok et al. (2011)]. As in previous works [Aubry, Thiam, Piel et al. (2014); Deveraux, Allena and Aubry (2017)], we model this contractility as an active strain through the decomposition of the deformation gradient tensor $\boldsymbol{F}$ as follows:

$$\boldsymbol{F} = \boldsymbol{F}_e \boldsymbol{F}_a \tag{2}$$

with $\boldsymbol{F}_e$ and $\boldsymbol{F}_a$ the elastic and active deformation gradient tensors, respectively. The deformation gradient is defined as $\boldsymbol{F} = \mathbf{I} + \mathbf{D_p u}$, where $\mathbf{D_p u}$ is the gradient of the displacement $\boldsymbol{u}$ with respect to the initial configuration $\mathbf{p}$. From here on, we put ourselves in the small deformation hypothesis. Indeed, although the overall strain of the cell is not small, it may be considered as the combination of successive small deformations, thus making such a hypothesis acceptable. We can assume that $\boldsymbol{F}_a$ is close to the identity and thus approximate it by $\boldsymbol{F}_a = \mathbf{I} + \boldsymbol{\omega}_a + \boldsymbol{\epsilon}_a$ where $\boldsymbol{\omega}_a$ is the anti-symmetric part of $\boldsymbol{F}_a$ that defines the rotation and $\boldsymbol{\epsilon}_a$ is the symmetric part of $\boldsymbol{F}_a$ that defines the strain.

From Eq. (2), we can then write:

$$\boldsymbol{F}_e = \boldsymbol{F}.\boldsymbol{F}_a^{-1} = (\mathbf{I} + \mathbf{D_x u})(\mathbf{I} - \boldsymbol{\omega}_a - \boldsymbol{\epsilon}_a) \tag{3}$$

Thus, the Green-Lagrange tensor $\boldsymbol{E}_e$ defined as $\boldsymbol{E} = \frac{1}{2}(\boldsymbol{F}^T.\boldsymbol{F} - \mathbf{I})$ reads:

$$\begin{aligned} \boldsymbol{E}_e &= \frac{1}{2}[(\mathbf{I} - \boldsymbol{\omega}_a - \boldsymbol{\epsilon}_a)^T (\mathbf{I} + \mathbf{D_x u})^T (\mathbf{I} + \mathbf{D_x u})(\mathbf{I} - \boldsymbol{\omega}_a - \boldsymbol{\epsilon}_a) - \mathbf{I}] \\ &= \frac{1}{2}(\mathbf{D_x u} + \mathbf{D_x u}^T - (\boldsymbol{\omega}_a + \boldsymbol{\omega}_a^T - 2\boldsymbol{\epsilon}_a) \end{aligned} \tag{4}$$

The cell's strain is defined as $\boldsymbol{\epsilon} = \frac{1}{2}(\mathbf{D_x u} + \mathbf{D_x u}^T)$ and, in the hypothesis of small deformations, we eventually come up with:

$$\boldsymbol{\epsilon}_e = \boldsymbol{\epsilon} - \boldsymbol{\epsilon}_a \tag{5}$$

with $\boldsymbol{\epsilon}_e$ and $\boldsymbol{\epsilon}_a$ the elastic and the active cell strains, respectively.

Then, the constitutive mechanical law reads:

$$\boldsymbol{\sigma'} = \lambda Tr(\boldsymbol{\epsilon} - \boldsymbol{\epsilon}_a)\mathbf{I} + 2\mu(\boldsymbol{\epsilon} - \boldsymbol{\epsilon}_a) \tag{6}$$

with λ and μ the Lamé coefficients of the solid part, defined as $\lambda = \frac{E\nu}{(1+\nu)(1-2\nu)}$ and $\mu = \frac{E}{2(1+\nu)}$, where E and ν are the Young modulus and the Poisson's ratio of the solid phase, respectively and Tr the trace operator.

If the cell is confined in a horizontal micro-channel, we can assume that the role of the gravity will be minimal. Experimental work moreover proved that gravity does not influence the active mechanism of cell spreading in a micro-pillars assay [Pan, Yan, Peng et al. (2012)].Since no volume forces are applied to the system, the cell fluid equilibrium equation then reads

$$\mathbf{Div}(\boldsymbol{\sigma}' - p_f \mathbf{I}) = \rho \mathbf{a} \tag{7}$$

where $\mathbf{Div}$ is the divergence and $\mathbf{a}$ is the acceleration, which is low but nonetheless relevant, at least from a numerical point of view. ρ is the weighted density defined as $\rho = \phi\rho_f + (1-\phi)\rho_s$, with ϕ the porosity of the cytoplasm, ρ_f the density of the interstitial fluid and ρ_s the density of the solid phase.

In order to model the fluid-solid interaction, we write down the mass conservation for each phase of the material locally. At such scale, the local quantities are marked with an asterisk and from the mass conservation of each phase, we can write [Bear and Bachmat (1990); Coussy (1995)]:

$$\begin{aligned} c_{p,s}\frac{dp_s^*}{dt} + div(\boldsymbol{v}_s^*) = 0 \\ c_{p,f}\frac{dp_f^*}{dt} + div(\boldsymbol{v}_f^*) = 0 \end{aligned} \tag{8}$$

with $c_{p,s}$ and $c_{p,f}$ the compressibility of the solid and the fluid phase respectively. p_s^* and p_f^* are the local pressures $\boldsymbol{v}_s^*$ and $\boldsymbol{v}_f^*$ are the local velocities. The subscripts s and f stand for solid and fluid, respectively.

We perform a volume integration on a representative volume element (RVE) Ω of total volume V_t, composed of a solid phase Ω_s of volume V_s and a fluid phase Ω_f of volume V_f (see Fig. 1), to get a homogenized problem.

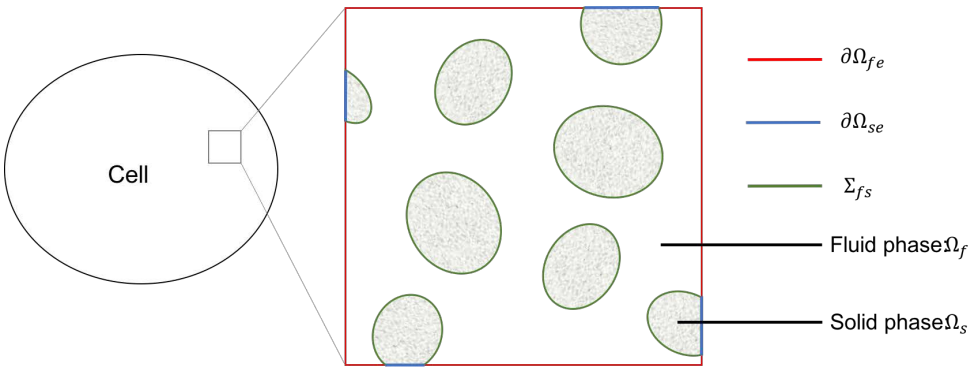

Figure 1: Illustration of the poroelastic system

$\partial\Omega_{se}$ and $\partial\Omega_{fe}$ are the exterior solid and fluid boundaries of the RVE, so that the total boundary $\partial\Omega_e = \partial\Omega_{se} \cup \partial\Omega_{fe}$. $\boldsymbol{n}_s$ and $\boldsymbol{n}_f$ are the outward normal vectors to each phase. The homogenized quantities are noted without the asterisk and we have:

$$\int_{\Omega_s}(c_{p,s}\frac{dp_s^*}{dt}+div(\boldsymbol{v}_s^*))\mathrm{d}V+\int_{\Omega_f}(c_{p,f}\frac{dp_f^*}{dt}+div(\boldsymbol{v}_f^*))\mathrm{d}V=0 \tag{9}$$

which gives

$$c_{p,s}\frac{dp_s}{dt}V_s+c_{p,f}\frac{dp_f}{dt}V_f+\int_{\Omega_s}div(\boldsymbol{v}_s^*)\mathrm{d}V+\int_{\Omega_f}div(\boldsymbol{v}_f^*)\mathrm{d}V=0 \tag{10}$$

The Stokes theorem allows us to write:

$$\begin{aligned}c_{p,s}\frac{dp_s}{dt}V_s+c_{p,f}\frac{dp_f}{dt}V_f+\int_{\partial\Omega_{se}}(\boldsymbol{v}_s^*,\boldsymbol{n}_s)\mathrm{d}S+\int_{\Sigma_{fs}}(\boldsymbol{v}_f^*,\boldsymbol{n}_f)\mathrm{d}S\\+\int_{\partial\Omega_{fe}}(\boldsymbol{v}_f^*,\boldsymbol{n}_f)\mathrm{d}S+\int_{\Sigma_{fs}}(\boldsymbol{v}_s^*,\boldsymbol{n}_s)\mathrm{d}S=0\end{aligned} \tag{11}$$

where $(\boldsymbol{a},\boldsymbol{b})$ indicates the scalar product of two vectors $\boldsymbol{a}$ and $\boldsymbol{b}$.
On Σ_{fs}, $\boldsymbol{n}_s=-\boldsymbol{n}_f$ and $\boldsymbol{v}_s=\boldsymbol{v}_f$, so $\int_{\Sigma_{fs}}(\boldsymbol{v}_f^*,\boldsymbol{n}_f)\mathrm{d}S+\int_{\Sigma_{fs}}(\boldsymbol{v}_s^*,\boldsymbol{n}_s)\mathrm{d}S=0$. The previous equation then becomes

$$c_{p,s}\frac{dp_s}{dt}V_s+c_{p,f}\frac{dp_f}{dt}V_f+\int_{\partial\Omega_e}(\boldsymbol{v}_s^*,\boldsymbol{n}_s)\mathrm{d}S+\int_{\partial\Omega_{fe}}(\boldsymbol{v}_f^*-\boldsymbol{v}_s^*,\boldsymbol{n}_f)\mathrm{d}S=0 \tag{12}$$

By applying the Stokes theorem the other way around and dividing everything by V_t, we introduce the porosity of the cytoplasm $\phi=\frac{V_f}{V_t}$ and we can write

$$\begin{aligned}c_{p,s}(1-\phi)\frac{dp_s}{dt}+c_{p,f}\phi\frac{dp_f}{dt}V_f+\frac{1}{V_t}\int_{\Omega}div(\boldsymbol{v}_s^*)\mathrm{d}V\\+\frac{1}{V_t}\int_{\partial\Omega_{fe}}(\boldsymbol{v}_f^*-\boldsymbol{v}_s^*,\boldsymbol{n}_f)\mathrm{d}S=0\end{aligned} \tag{13}$$

$\frac{1}{V_t}\int_{\Omega}div(\boldsymbol{v}_s^*)\mathrm{d}V$ is the solid matrix deformation so $\frac{1}{V_t}\int_{\Omega}div(\boldsymbol{v}_s^*)\mathrm{d}V=Tr(\dot{\epsilon})$. The application of the Stokes theorem allows to rewrite the equation as:

$$c_{p,s}(1-\phi)\frac{dp_s}{dt}+c_{p,f}\phi\frac{dp_f}{dt}+Tr(\dot{\epsilon})+div(\boldsymbol{v}_f-\boldsymbol{v}_s)=0 \tag{14}$$

Additionally, the Darcy equation of fluid flow in porous media reads:

$$\boldsymbol{v}_f-\boldsymbol{v}_s=-\frac{1}{\eta_f}\mathbf{K}_f(\nabla p_f) \tag{15}$$

where η_f is the fluid viscosity, $\mathbf{K}_f$ is the fluid intrinsic permeability matrix and ∇ is the gradient operator.

By combining Eqs. (14) and (15), we get the global poroelastic equation of our model:

$$c_{p,s}(1-\phi)\frac{dp_s}{dt}+c_{p,f}\phi\frac{dp_f}{dt}+Tr(\dot{\epsilon})+div(-\frac{1}{\eta_f}\mathbf{K}_f(\nabla p_f))=0 \tag{16}$$

2.2 Reduction to a 1D problem

In our model, we choose to represent the cell as 1D element in the *x* direction. To do so, we average a 2D model in the other direction:

$$\bar{f} = \frac{1}{H}\int_{-H/2}^{H/2} f(z)\mathrm{d}z \tag{17}$$

where $\bar{f}$ defines the average of a function f and H is the height of the cell in the *z* direction. Eq. (1) then becomes:

$$\bar{\sigma}_{xx} = (\lambda+2\mu)(\bar{\epsilon}_{xx}-\bar{\epsilon}_a) - \bar{p}_f = (\lambda+2\mu)(\frac{\partial \bar{u}}{\partial x} - \bar{\epsilon}_a) - \bar{p}_f \tag{18}$$

where u is the displacement along the *x*-axis.

The integration of Eq. (7) along the *z*-axis

gives:

$$\rho\frac{\partial^2 \bar{u}}{\partial t^2} = \frac{\partial \bar{\sigma}_{xx}}{\partial x} + \sigma_{xz}(\frac{H}{2}) - \sigma_{xz}(-\frac{H}{2}) \tag{19}$$

By combining these last two equations, we find:

$$\rho\frac{\partial^2 \bar{u}}{\partial t^2} - (\lambda+2\mu)(\frac{\partial^2 \bar{u}}{\partial x^2} - \frac{\partial \bar{\epsilon}_a}{\partial x}) = -\frac{\partial \bar{p}}{\partial x} + \bar{\tau} \tag{20}$$

with $\bar{\tau} = \frac{1}{H}(\sigma_{xz}(\frac{H}{2}) - \sigma_{xz}(-\frac{H}{2}))$ the weighted shear stress.

In the global poroelastic Eq. (16), we assume that we can neglect the solid phase compress-ibility so that the final equation then reads:

$$c_{p,f}\phi\frac{\partial \bar{p}_f}{\partial t} + \frac{\partial}{\partial t}\frac{\partial \bar{u}}{\partial x} = k\frac{\partial^2 \bar{p}_f}{\partial x^2} \tag{21}$$

where $k = \frac{K_f}{\eta_f}$ is the effective permeability, K_f being the scalar version of $\mathbf{K}_f$ due to the 1D reduction.

Boundary conditions. Here, the cell membrane is not permeable to outside fluid. We choose this hypothesis as a first approximation, even though we are aware of the importance of water permeation in cells [Murata, Mitsuoka, Hirai et al. (2000)], in order to build a first model that shall later be improved. Then, the boundary conditions on the fluid at both ends of the cell read $K_f \nabla \bar{p}_f = 0$. From a mechanical point of view, the outside fluid pressure is negligible so that $\sigma_{xx} = 0$ at both ends. Besides, we consider the cell to be at rest at the initial time $t = 0$.

2.3 The Coulomb's friction law

The ability of the cell to progress in confinement is linked to the f riction g enerated by the cell in contact with the confining surface. Assuming that the contact is established between the cell and the confining surface, the Coulomb's friction-sliding law reads [Coulomb (1821); Pfeiffer (2008)]:

$$\frac{\partial \bar{u}}{\partial t} = \begin{cases} 0 & \text{if } |\bar{\tau}| < \mu_f |\bar{\sigma}_{zz}| \text{ stick phase} \\ -\lambda_c \bar{\tau} & \text{if } |\bar{\tau}| = \mu_f |\bar{\sigma}_{zz}| \text{ slip phase} \end{cases} \tag{22}$$

with λ_c a scalar and μ_f the friction coefficient.
Then, in the slipping phase, we can write

$$\lambda_c = \frac{|\frac{\partial \bar{u}}{\partial t}|}{|\bar{\tau}|}$$

As a result,

$$\bar{\tau} = -|\bar{\tau}| \frac{\frac{\partial \bar{u}}{\partial t}}{|\frac{\partial \bar{u}}{\partial t}|}$$

Eventually,

$$\bar{\tau} = -\mu_f |\bar{\sigma}_{zz}| \frac{\frac{\partial \bar{u}}{\partial t}}{|\frac{\partial \bar{u}}{\partial t}|}$$

Besides, if we assume that the strain in the *z*-direction is negligible, we can write $\sigma_{zz} = -p_f$
All in all, we obtain

$$\bar{\tau} = -\mu_f |\bar{p}_f| \frac{\frac{\partial \bar{u}}{\partial t}}{|\frac{\partial \bar{u}}{\partial t}|} = -\mu_f |\bar{p}_f| sign(\frac{\partial \bar{u}}{\partial t}) \tag{23}$$

with $sign(\cdot)$ the sign function.
This force can be described in Fig. 2.
As we can see, the classical difficulty with Coulomb's law is that it is not a continuous function. For a zero velocity, there are infinite values for $\bar{\tau}$ and if $\bar{\tau}$ reaches its threshold, there is no way to determine the velocity. In order to solve this issue, we use a regularized sign function .
The regularized Coulomb's law reads [Aström and Canudas de Wit (2008)]:

$$\bar{\tau} = -\mu_f |\bar{p}_f| smsign(\frac{\partial \bar{u}}{\partial t}) \tag{24}$$

where $|\bar{\sigma}_{zz}| = |\bar{p}_f|$ if we consider that the strain occurs solely in the x direction. $smsign(\cdot)$ is the regularized form of the sign function.In this respect the shear stress is always smaller than $\mu_f |\bar{p}_f|$ with a vanishing velocity and very close to $\mu_f |\bar{p}_f|$ when the sliding velocity is larger. This smoothed sliding friction has often been used in non linear dynamical or mechanical systems. It requires only one parameter and it generates stable, efficient and fast computations.

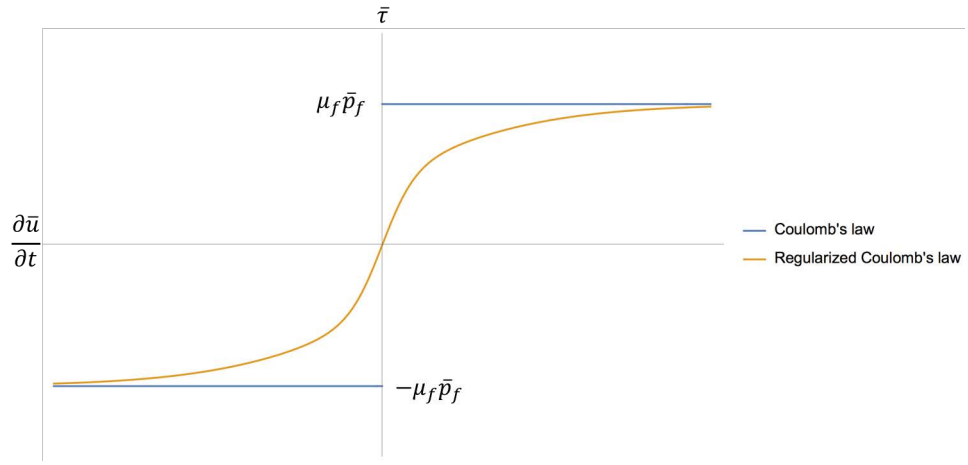

Figure 2: Diagram of the Coulomb's friction force and its regularized form

2.4 Active strain

Cells that use bleb-based migration present a very particular type of active deformation. Indeed, this migration mode does not require actin polymerization, but solely relies on cyclic myosin-driven contractility in the uropod, the cell's rear. In our model, the active strain $\bar{\epsilon}_a(x,t)$ is written as a time periodic function (see Fig. 3) of period T_0, spatially localized $\forall x \in [x_0 - \frac{dx_0}{2}; x_0 + \frac{dx_0}{2}]$, as follows, with x_0 and dx_0 geometrical parameters defining the active strain zone in the cell:

$$\bar{\epsilon}_a(x,t) = -e_{a,0}(h(t - t_{0,up}, s) - h(t - t_{0,down}, s)) \; \forall x \in [x_0 - \frac{dx_0}{2}; x_0 + \frac{dx_0}{2}] \tag{25}$$

where $e_{a,0}$ is the amplitude, $t_{0,cont}$ and $t_{0,decont}$ describe the time at which the contraction/decontraction occurs and s_a regulates the slope of the active strain.

The relatively fast contraction and decontraction, over a time of 4 s, was chosen so that the resulting pressure would be high enough for the creation of a bleb. The value of T_0, 30 s, to fit the blebbing time scale found in the literature [Charras and Paluch (2008)].

2.5 Blebbing and Young's modulus

Bleb initiation starts from the weakening of bonds between the actin cortex and the cell membrane. The bleb then grows until such bonds are reformed, thus stabilizing the bleb. In order to model this local weakening, we chose a quite raw approximation to begin with: The cell's Young's modulus E_{cell} is locally weakened at the cell front, which enables easier blebbing, such that

$$E_{cell} = \begin{cases} E_{cell,0} & \text{if } x < \frac{3}{4} L_{cell} \\ (1-D) E_{cell,0} & \text{if } x \geq \frac{3}{4} L_{cell} \end{cases} \tag{26}$$

where $E_{cell,0}$ is the un-damaged cell's Young's modulus, L_{cell} is the cell's dimension and D is the damage coefficient.

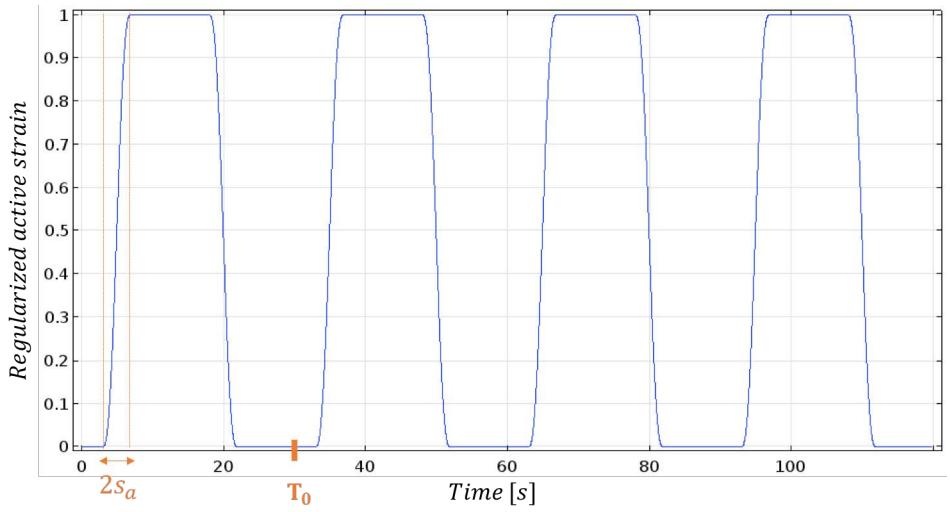

Figure 3: Graphical representation of the regularized active strain during four cycles of 30 s each

To sum up, our poroelastic model rests on three main features: The active strain, as described in Eq. (25), the poroelastic laws of the model, that summed up in Eqs. (20) and (21), and the self-synchronized friction law, described in its final form in Eq. (26).

3 Results

In this section, we present the results of our 1D model, implemented in COMSOL Multiphysics©. The contractile zone at the rear of the cell and the blebbing front zone are both 5 μm long. The description and value of each parameter are listed in Tab. 1. We use quadratic finite elements for the displacement variable and linear elements for the intracellular pressure to prevent mesh locking phenomena. The mesh is a 1D uniform one with a discretization length of 0.5 μm. In the solver parameters, a fifth degree Backwards Euler integration is employed and at each time step, a Newton method is used with a relative tolerance of 0.01 with regards to both fields. A computational run for 120 s physical time takes about 3 min CPU time.

Table 1: Values and description of the model's parameters

Parameter	Description	Value (unit)	References
L_{cell}	Cell dimension	20 μm	
$E_{cell,0}$	Cell Young's modulus	1 kPa	Kuznetsova, Staro-dubtseva, Yegorenkov et al. (2007)
D	Damage coefficient	0.9	

ρ	Weighted cell density	1000 kg/m^3	
k	Effective permeability	$10^{-14}\, m^4/N.s$	Guilak, Haider, Set-ton et al. (2006)
$c_{p,f}$	Compressibility of the cell's fluid phase	$5 \times 10^{-4}\ Pa^{-1}$	
ϕ	Cytoplasm porosity	0.5	Taber, Shi, Yang et al. (2011)
μ_f	Friction coefficient	0.3	
$e_{a,0}$	Amplitude of the active strain	0.8	
x_0	Geometrical parameter of the active strain	2.5 μm	
dx_0	Geometrical parameter of the active strain	5 μm	
T_0	Period of the active strain	30 s	Charras and Paluch (2008)
$t_{0,up}$	Temporal parameter of the active strain	5 s	
$t_{0,down}$	Temporal parameter of the active strain	20 s	
s_a	Temporal parameter of the active strain	2 s	

We first show that the friction force leads to a self synchronization that enables a net cell motion forward. Then, we proceed to a sensibility analysis to identify the key parameters that determine the ability of the cell to successfully migrate, and to study the influence of the secondary parameters on the migration speed.

3.1 A successful synchronization and the cell migrates

A new point tackled by this model is that no adhesion is required for the cell to move forward. Moreover, what gets really interesting is that the synchronization between the Coulomb's friction force and the cell motion is self-determined. In fact, there is no need for a synchronization function, as it was the case in our previous works [Deveraux, Allena and Aubry (2017); Aubry, Thiam, Piel et al. (2014); Allena (2014)], and mechanics alone regulates this interaction.

We perform an analysis of our model on 4 periods of active strain (i.e. 120 s). The first contraction cycle shows a different behaviour from the following ones and can be seen as a necessary step to reach a new dynamic equilibrium. Then, the further analyses will be made excluding this initial cycle. Obviously, in the absence of friction (μ_f=0), the cell pulsates on place but does not move forward. This configuration is interesting to study the poroelastic part of the model. Indeed, we observe a lag time between the displacement of the cell rear, due to the active contraction, and the one of the cell front, that is a direct consequence of poroelasticity. Plotting the displacement of the cell front and rear rather

than their position, which would simply induce an offset of the front, allows to spot more easily if the cell is overall contracted or extended (see Fig. 4a). Besides, the intra-cellular pressure p_f is transported towards the front of the cell over one period of active strain (see Fig. 4b), which enables the development of a frontal bleb. Due to blebbing, the pressure does not have time to build up at the front, which explains the low values compared to the pressure at the rear (30 Pa at the front *vs.* 400 Pa at the rear).

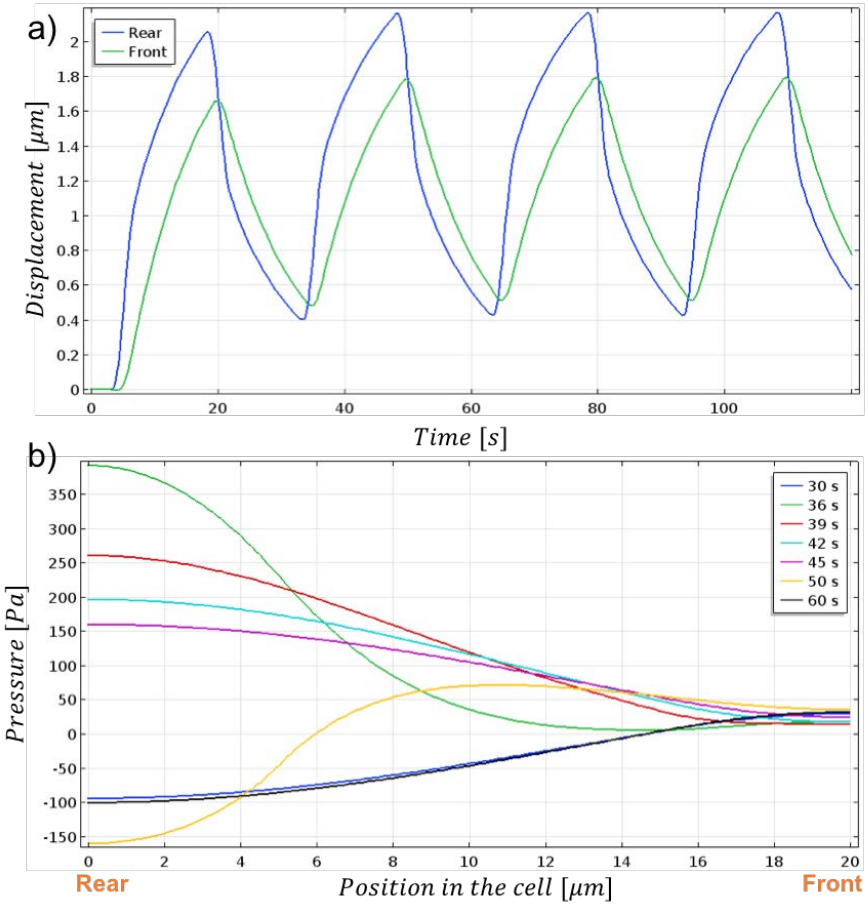

Figure 4: Graphical representation of a) the displacement of the rear (blue) and front (green) extremities of the cell over four periods of active strain and b) the intra-cellular pressure along the cell length over one period of active strain

3.1.1 Poroelasticity enables cell blebbing

After pointing out the influence of poroelasticity, the full model is studied, now including the friction force with μ_f=0.3. First, the pressure evolution inside the cell does not change from the previous case, which is not surprising since poroelasticity occurs in the same way. However, the displacement of the cell is strongly impacted (see Fig. 5). The lag between the displacement of the rear and front of the cell is very similar to the previous

case, but a net forward motion of the cell of 2 μm for the first cycle, and then 4 μm per cycle occurs. The cell migrates at an average speed of 8 $\mu m/min$, which is in the range of the values experimentally found for blebbing cells in confinement [Ibo, Srivastava, Robinson et al. (2016); Liu, Le Berre, Lautenschlaeger et al. (2015); Yip, Chiam and Matsudaira (2015)].

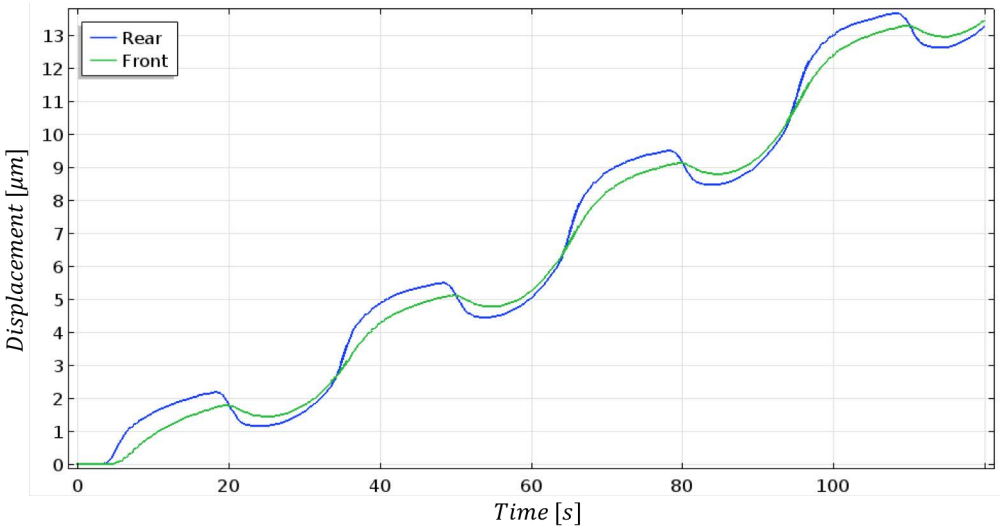

Figure 5: Graphical representation of the displacement of the rear (blue) and front (green) extremities of the cell over three periods of active strain

3.1.2 The fine action of the friction force

Once made sure that our poroelastic model does enable bleb formation, we need to take it to the next step and find the parameters that will generate a net forward motion, which is the goal of the Coulomb's friction force. To do so, we first integrate the friction force over the whole cell to study the total force F_{tot} applied to the cell. When F_{tot} is negative, it generally prevents a forward motion and, when negative, it prevents a backward motion. During cycle 2 (and the following ones), two events need to be addressed: First a negative peak of -1.45 nPa at 35.5 s, a positive rise up to 0.7 nPa from 55 s to the end of the cycle (see Fig. 6). However, this global view conceals the local phenomena, which are of great interest here in order to pinpoint where the friction is the strongest.

To do so, we study the first peak at t=35.5 s corresponding to the contraction and the time period from 55 s to 60 s -right after decontraction-and plot the friction force $\bar{\tau}$ along the cell length every second from 55 s to 60 s. During contraction, there is a strong friction at the uropod which is the direct consequence of the rear shrinkage. Indeed, the friction is negative from 0 µm to 4 μm and positive from 4 µm to 7 μm (see Fig. 7a). The cell is then mostly blocked from moving forward because the negative part of $\bar{\tau}$ is much stronger than the positive one. If we focus on what occurs after the decontraction however, the picture is quite different. As time progresses, $\bar{\tau}$ increases in the positives at the rear and slightly decreases in the negatives at the front (see Fig. 7 b).

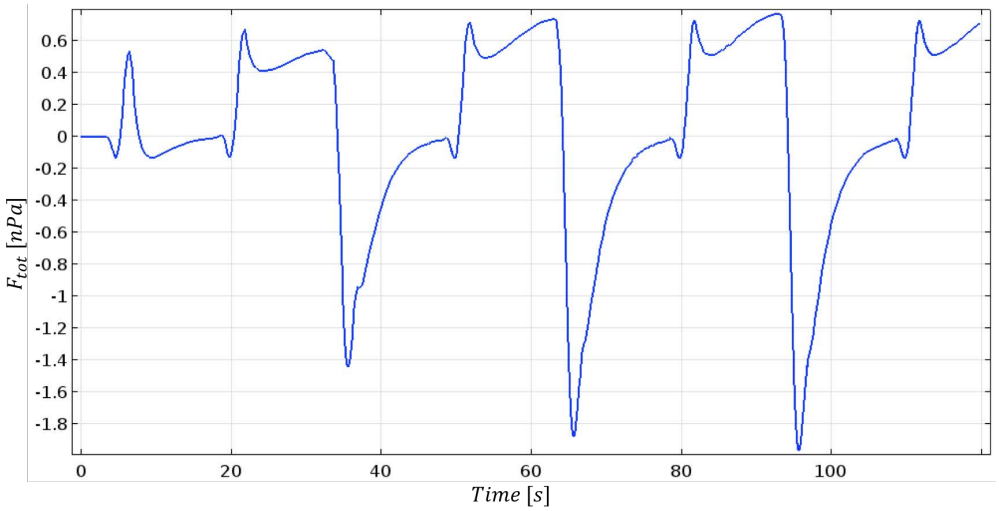

Figure 6: Graphical representation of the total force applied to the cell

This means that the friction necessary for the cell to move forward is mostly located in the rear part of the cell and not at the bleb, as it has been suggested in exploratory works on blebbing migration [Charras and Paluch (2008)].

These results are very interesting since they offer a completely mechanics-based insight of chimneying. In fact, although often observed, this phenomenon is quite unclear from the mechanical point of view. Hypotheses were made that the cell pushed against the confining walls, but no further mechanical inquiries were undertaken. Our model, although still preliminary, already unveils interesting mechanisms. First, it proves that a simple mechanical friction force is sufficient for the cell to move forward at a reasonable rate. Second, it reveals that the friction required for chimneying is located at the rear of the cell during the uropod decontraction.

3.2 Sensibility study

Now, we study the influence of the parameters on the cell behaviour. Some parameters are crucial to the migration, while others simply regulate its amplitude.

Then, the model's parameters can be divided into three categories:

Discriminating: They determine whether the cell migrates or not: μ_f, $c_{p,f}$, E_{cell}

Non-discriminating: They determine how fast the cell migrates: k, s_a

Technical: They purely define the problem: L_{cell}, ρ, ϕ, $e_{a,0}$, x_0, dx_0, T_0, $t_{0,up}$, $t_{0,down}$

3.2.1 The conditions for a successful synchronization

As seen in the Section 3.1, the friction is the corner stone of our model: Without it, no migration is possible. Intermediate values of the friction coefficient μ_f lead to intermediate migration speed, as could be expected (see Fig. 8a).

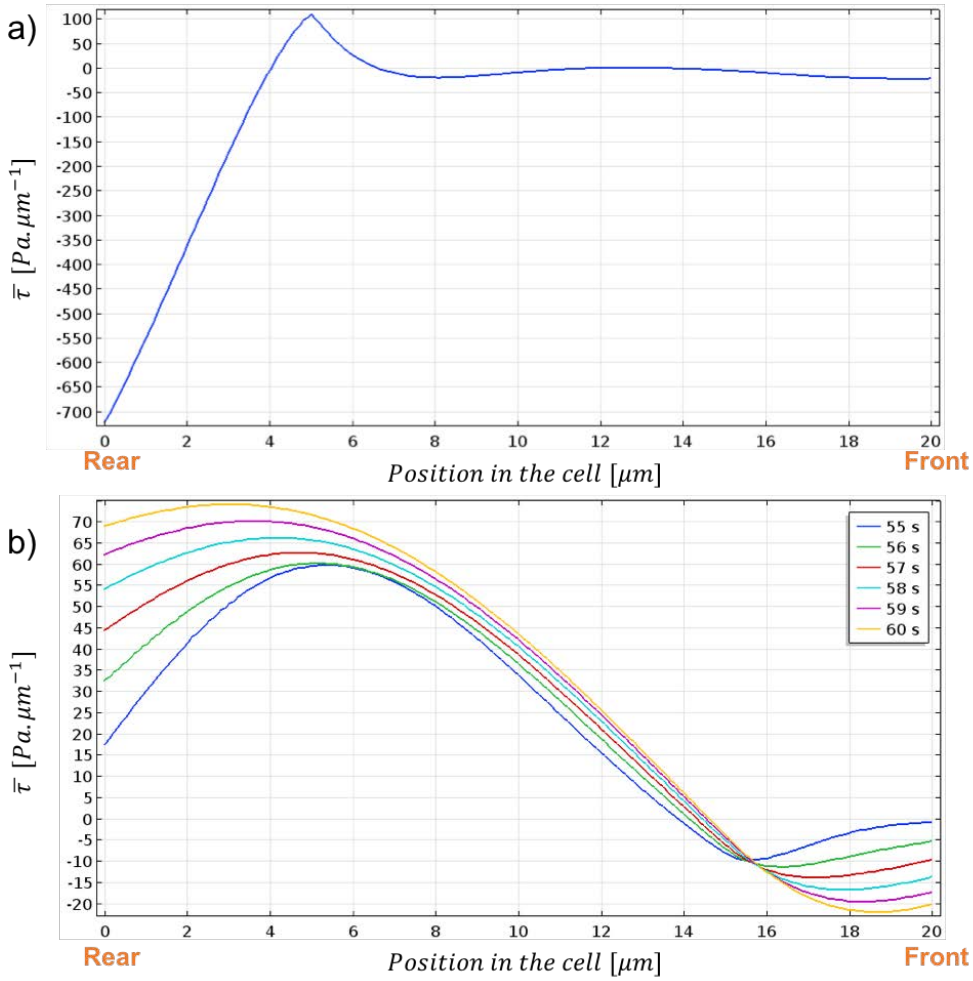

Figure 7: Graphical representation of a) friction force per unit length along the cell profile at t=35.5 s, b) friction force per unit length along the cell profile between 55 s and 60 s with a line every 3 s

The Young's modulus was chosen at 1 kPa. Each cell type has a different range of Young's modulus, making it interesting to study its influence on cell motility in the prospect of looking at specific cell types. There appears to be an optimum in cell displacement for E_{cell}=1000 Pa. For higher values, the migration speed decreases and at 5 kPa, the cell may even go in the opposite direction (see Fig. 8b). The decrease of the cell compressibility $c_{p,f}$ induces a faster migration but, more importantly, a too high compressibility leads to no migration or even a backward one (see Fig. 8c). In each case, this is due to an insufficient level of intra-cellular pressure mobilization with respect to the friction force.

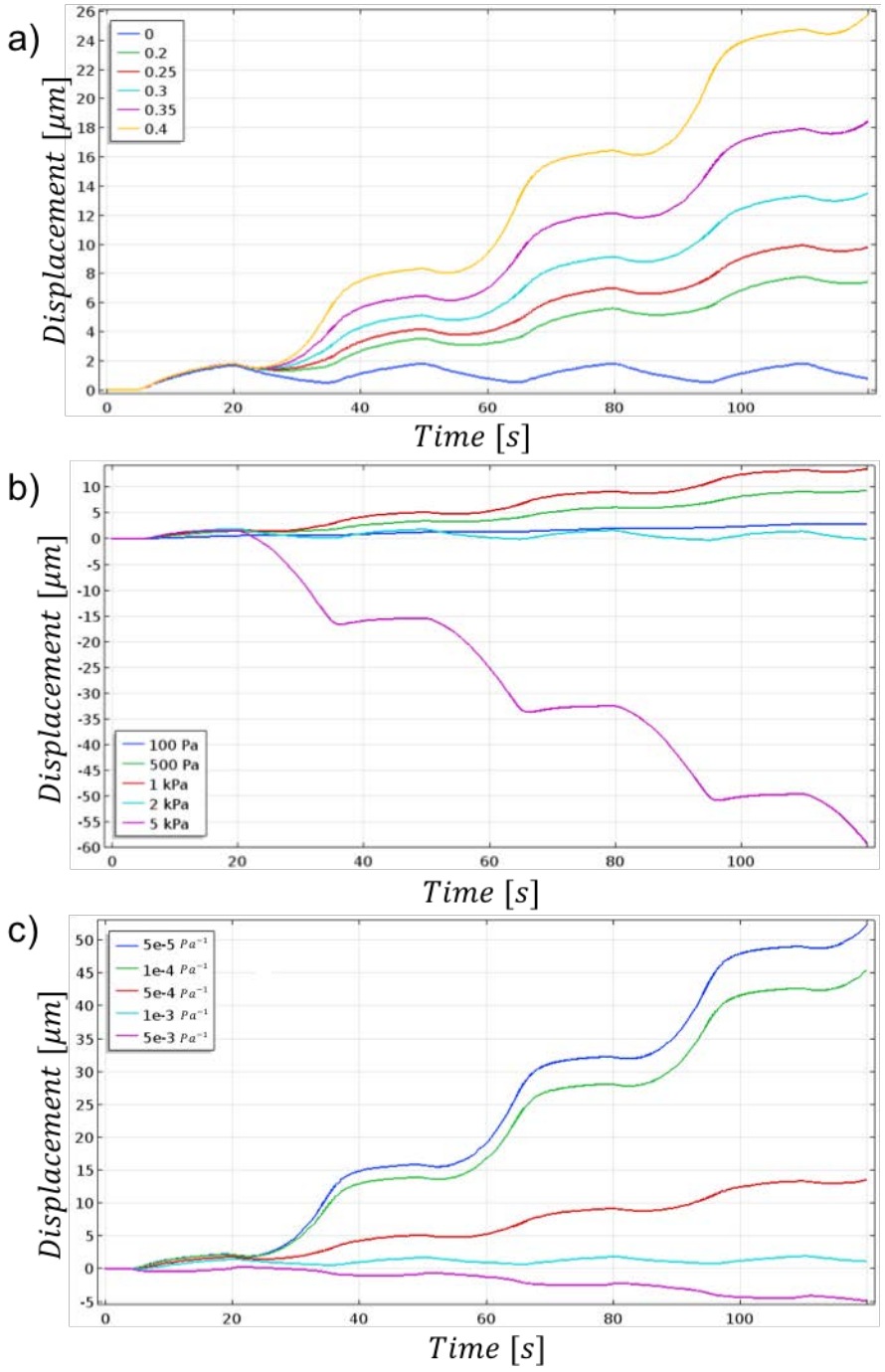

Figure 8: Cell front displacement-Parametric study on a) μ_f b) E_{cell} c) $c_{p,f}$

3.2.2 Sensitivity of the other parameters

The others parameters simply define how fast the cell migrates, but they do not influence the capacity of the cell to migrate. The rate of active strain, directly linked to s_a, influences

chimneying velocity: The faster it is (the lower s_a is), the faster the cell migrates (see Fig. 9a). Concerning the effective permeability k, we observe the same trend as for the Young's modulus, but we do not reach a backward migration.

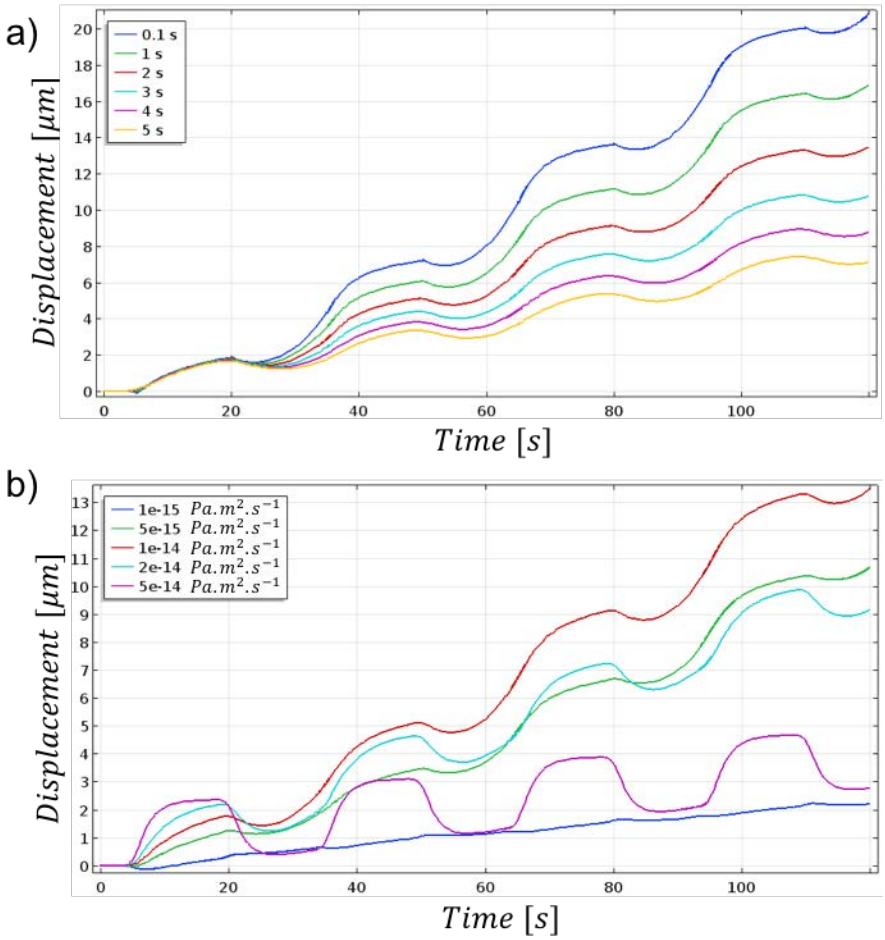

Figure 9: Cell front displacement-Sensibility study on a) s_a b) k

In order to get a new insight on our results, we introduce the so-called half-reduced time $t_{1/2} = \frac{L_{cell}^2}{2kE_{cell}}$. It gives an order of time needed to observe the poroelastic phenomenon. The values of $t_{1/2}$ for the values of the parameters tested in the parametric study are listed in Tab. 2.

From this table, we can see that the optimal migration speed occurs when $t_{1/2}$ is ten folds grater than s_a. Indeed, for greater values of $t_{1/2}$, there is no time for intra-cellular fluid flow to occur, and for the lowest values, the pressure does not have time to build up before the fluid leaves the cell rear. Since we saw that the friction force occurs at the rear of the cell, we understand that if there is no pressure increase, then the friction remains too low to enable migration. In the case of E_{cell}=5000 Pa, the friction force is too negative, and the cell goes the wrong way.

Table 2: Half-reduced time values for different parameters couples

$t_{1/2}$ (s)	$E_{cell}(Pa)$	k $(m^4/N.s)$
200	1000	10^{-15}
	100	10^{-14}
40	1000	5.10^{-15}
	500	10^{-14}
20	1000	10^{-14}
10	1000	2.10^{-14}
	2000	10^{-14}
4	1000	5.10^{-14}
	5000	10^{-14}

4 Discussion and conclusion

Our preliminary model presents very interesting insights on the combined role of poroelasticity and passive friction force during the migration mode known as chimneying. In this work, we focus on the sharp synchronization between poroelastic-based blebbing and passive friction force. In this respect, we chose to implement a 1D model of a generic cell which could be adapted to fit a specific cell type. This 1D reduction is of course a rough simplification that induces a loss of information, but it simplifies the problem and allows to pinpoint the exact mechanisms that govern chimneying. Finding out the values of the model's parameters was complex due to the lack of experimental data, or the wide range of the data that could be found. Thus, after starting with first-approximation values of the parameters from the literature, we iterated until getting an acceptable set of parameters for the model to run (see Tab. 1). The model's sensibility on cell stiffness highlights the various behaviour that could be expected from various cell types and it raises the question of the possibility of such migration mode in stiffer cells.

Despite the simplifications, there is still a lot to learn from our model. Our model rests on three pillars: Active contractility, a poroelastic material law, and the self-synchronized friction force. First, it shows the need for poroelasticity intra-cellular fluid flows in the pro-cess of blebbing. Indeed, the active contraction on the cell's uropod causes an increase of intra-cellular pressure at the rear that propagates through the cell. When the pressure wave reaches the mechanically weakened front of the cell, it induces a bleb growth. The last pillar is the self-synchronized friction force between the cell and the confining surface. Indeed, contrarily to our previous works [Deveraux, Allena and Aubry (2017); Aubry, Thiam, Piel et al. (2014)], the synchronization between the active strain and the force from the cell-environment interaction is completely self-determined, which is a major step towards a more autonomous model. Our model sheds light on the question of the location of the friction force needed for the cell to move forward: The force enabling migration is the strongest at the cell rear. These findings allow further research to focus its attention more specifically on the cell's uropod and experimentally investigate the molecular processes at stake there.

In order take this model further, we could consider more cellular components, which can

be described with specific constitutive properties by using spatial characteristic functions as in our previous works [Aubry, Thiam, Piel et al. (2014); Deveraux, Allena and Aubry (2017)]. The presence of the nucleus for instance could trigger interesting phenomena, such as a piston effect [Petrie, Koo and Yamada (2014)]. This exploratory model is only a proof of concept of future more complex versions that could be developed to study the influence of specific cell features in unhealthy cells. Indeed, blebbing is involved in various diseases such as cancer metastasis [Friedl (2004); Sahai and Marshall (2003)] or angiogenesis [Gebala, Collins, Geudens et al. (2016)] and our model could be adapted to these various cases to deepen our understanding of the mechanics of such phenomena.

Acknowledgement: This work was funded by a ministerial doctoral fellowship of the French Government.

References

Allena, R. (2013): Cell migration with multiple pseudopodia: Temporal and spatial sensing models. *Bulletin of Mathematical Biology*, vol. 75, no. 2, pp. 288-316.

Allena, R. (2014): Mechanical modelling of confined cell migration across constricted-curved micro-channels. *Molecular and Cellular Biomechanics*, vol. 11, no. 3, pp. 185-208.

Allena, R.; Aubry, D. (2012): A purely mechanical model to explore amoeboid cell migration. *Computer Methods in Biomechanics and Biomedical Engineering*, vol. 15, no. Supplement 1, pp. 14-16.

Allena, R.; Aubry, D. (2012): 'Run-and-tumble' or 'look-and-run'? A mechanical model to explore the behavior of a migrating amoeboid cell. *Journal of Theoretical Biology*, vol. 306, pp. 15-31.

Allena, R.; Aubry, D.; Sharpe, J. (2013): On the mechanical interplay between intra- and inter-synchronization during collective cell migration: A numerical investigation. *Bulletin of Mathematical Biology*, vol. 75, no. 12, pp. 2575-2599.

Arroyo, M.; Trepat, X. (2017): Hydraulic fracturing in cells and tissues: Fracking meets cell biology. *Current Opinion in Cell Biology*, vol. 44, no. Supplement C, pp. 1-6.

Aström, K. J.; Canudas de Wit, C. (2008): Revisiting the LuGre friction model. *IEEE Control Systems Magazine*, vol. 28, no. 6, pp. 101-114.

Aubry, D.; Thiam, H.; Piel, M.; Allena, R. (2014): A computational mechanics approach to assess the link between cell morphology and forces during confined migration. *Biomechanics and Modeling in Mechanobiology*, vol. 14, no. 1, pp. 143-157.

Bear, J.; Bachmat, Y. (1990): *Introduction to Modeling of Transport Phenomena in Porous Media*. Springer Netherlands, Dordrecht.

Cao, X.; Moeendarbary, E.; Isermann, P.; Davidson, P. M.; Wang, X. et **a**l**.** (2016): A chemomechanical model for nuclear morphology and stresses during cell transendothelial migration. *Biophysical Journal*, vol. 111, no. 7, pp. 1541-1552.

Charras, G.; Paluch, E. (2008): Blebs lead the way: How to migrate without lamellipodia. *Nature Reviews Molecular Cell Biology*, vol. 9, no. 9, pp. 730-736.

Chhabra, E. S.; Higgs, H. N. (2007): The many faces of actin: Matching assembly factors with cellular structures. *Nature Cell Biology*, vol. 9, no. 10, pp. 1110-1121.

Coulomb, C. A. (1821): *Théorie Des Machines Simples*. Bachelier, Paris.

Coussy, O. (1995): *Mechanics of Porous Continua*. Wiley, Chichester, New York.

Cowin, S. C. (1999): Bone poroelasticity. *Journal of Biomechanics*, vol. 32, no. 3, pp. 217-238.

Deveraux, S.; Allena, R.; Aubry, D. (2017): A numerical model suggests the interplay between nuclear plasticity and stiffness during a perfusion assay. *Journal of Theoretical Biology*, vol. 435, pp. 62-77.

Friedl, P. (2004): Prespecification and plasticity: Shifting mechanisms of cell migration. *Current Opinion in Cell Biology*, vol. 16, no. 1, pp. 14-23.

Gebala, V.; Collins, R.; Geudens, I.; Phng, L.-K.; Gerhardt, H. (2016): Blood flow drives lumen formation by inverse membrane blebbing during angiogenesis *in vivo*. *Nature Cell Biology*, vol. 18, no. 4, pp. 443-450.

Ghosh, S.; Ozcelikkale, A.; Dutton, J. C.; Han, B. (2016): Role of intracellular poroelasticity on freezing-induced deformation of cells in engineered tissues. *Journal of the Royal Society Interface*, vol. 13, no. 123.

Guilak, F.; Haider, M. A.; Setton, L. A.; Laursen, T. A.; Baaijens, F. P. T. (2006): Multiphasic models of cell mechanics. In Mofrad, M. R. K.; Kamm, R. D. (Eds): *Cytoskeletal Mechanics*, pp. 84-102. Cambridge University Press, Cambridge.

Hawkins, R. J.; Piel, M.; Faure-Andre, G.; Lennon-Dumenil, A. M.; Joanny, J. F. et al. (2009): Pushing off the walls: A mechanism of cell motility in confinement. *Physical Review Letters*, vol. 102, no. 5.

Henrichsen, J. (1972): Bacterial surface translocation: A survey and a classification. *Bacteriological Reviews*, vol. 36, no. 4, pp. 478-503.

Ibo, M.; Srivastava, V.; Robinson, D. N.; Gagnon, Z. R. (2016): Cell blebbing in confined microfluidic environments. *PloS One*, vol. 11, no. 10.

Kappe, S. H. I.; Buscaglia, C. A.; Bergman, L. W.; Coppens, I.; Nussenzweig, V. (2004): Apicomplexan gliding motility and host cell invasion: Overhauling the motor model. *Trends in Parasitology*, vol. 20, no. 1, pp. 13-16.

Karcher, H.; Lammerding, J.; Huang, H.; Lee, R. T.; Kamm, R. D. et al. (2003): A three-dimensional viscoelastic model for cell deformation with experimental verification. *Biophysical Journal*, vol. 85, no. 5, pp. 3336-3349.

Kuznetsova, T. G.; Starodubtseva, M. N.; Yegorenkov, N. I.; Chizhik, S. A.; Zhdanov, R. I. (2007): Atomic force microscopy probing of cell elasticity. *Micron*, vol. 38, no. 8, pp. 824-833.

Lim, F. Y.; Koon, Y. L.; Chiam, K. H. (2013): A computational model of amoeboid cell migration. *Computer Methods in Biomechanics and Biomedical Engineering*, vol. 16, no. 10, pp. 1085-1095.

Liu, Y. J.; Le Berre, M.; Lautenschlaeger, F.; Maiuri, P.; Callan-Jones, A. et al. (2015): Confinement and low adhesion induce fast amoeboid migration of slow mesenchymal cells. *Cell*, vol. 160, no. 4, pp. 659-672.

Lämmermann, T.; Bader, B. L.; Monkley, S. J.; Worbs, T.; Wedlich-Säldner, R. et al. (2008): Rapid leukocyte migration by integrin-independent flowing and squeezing. *Nature*, vol. 453, no. 7191, pp. 51-55.

Lorentzen, A.; Bamber, J.; Sadok, A.; Elson-Schwab, I.; Marshall, C. J. (2011): An ezrin-rich, rigid uropod-like structure directs movement of amoeboid blebbing cells. *Journal of Cell Science*, vol. 124, no. 8, pp. 1256-1267.

Malawista, S. E.; de Boisfleury Chevance, A.; Boxer, L. A. (2000): Random locomotion and chemotaxis of human blood polymorphonuclear leukocytes from a patient with Leukocyte Adhesion Deficiency-1: Normal displacement in close quarters via chimneying. *Cell Motility and the Cytoskeleton*, vol. 46, no. 3, pp. 183-189.

Maugis, B.; Brugués, J.; Nassoy, P.; Guillen, N.; Sens, P. et al. (2010): Dynamic insta-bility of the intracellular pressure drives bleb-based motility. *Journal of Cell Science*, vol. 123, no. 22, pp. 3884-3892.

Moeendarbary, E.; Valon, L.; Fritzsche, M.; Harris, A. R.; Moulding, D. A. et al. (2013): The cytoplasm of living cells behaves as a poroelastic material. *Nature Materials*, vol. 12, no. 3, pp. 253-261.

Murata, K.; Mitsuoka, K.; Hirai, T.; Walz, T.; Agre, P. et al. (2000): Structural determinants of water permeation through aquaporin-1. *Nature*, vol. 407, no. 6804, pp. 599-605.

Paluch, E. K.; Raz, E. (2013): The role and regulation of blebs in cell migration. *Current Opinion in Cell Biology*, vol. 25, no. 5, pp. 582-590.

Pan, Z.; Yan, C.; Peng, R.; Zhao, Y.; He, Y. et al. (2012): Control of cell nucleus shapes via micropillar patterns. *Biomaterials*, vol. 33, no. 6, pp. 1730-1735.

Pena, A.; Bolton, M. D.; Pickard, J. D. (1998): Cellular poroelasticity: A theoretical model for soft tissue mechanics. *Proceedings of the Biot Conference on Poromechanics*, pp. 475-480.

Petrie, R. J.; Koo, H.; Yamada, K. M. (2014): Generation of compartmentalized pressure by a nuclear piston governs cell motility in a 3D matrix. *Science*, vol. 345, no. 6200, pp. 1062-1065.

Pfeiffer, F. (2008): *Mechanical System Dynamics*. Berlin Springer.

Sahai, E.; Marshall, C. J. (2003): Differing modes of tumour cell invasion have distinct requirements for Rho/ROCK signalling and extracellular proteolysis. *Nature Cell Biology*, vol. 5, no. 8, pp. 711-719.

Silflow, C. D.; Lefebvre, P. A. (2001): Assembly and motility of eukaryotic cilia and flagella. Lessons from Chlamydomonas reinhardtii. *Plant Physiology*, vol. 127, no. 4, pp. 1500-1507.

Stroka, K. M.; Jiang, H.; Chen, S. H.; Tong, Z.; Wirtz, D. et al. (2014): Water permeation drives tumor cell migration in confined microenvironments. *Cell*, vol. 157, no. 3, pp. 611-623.

Strychalski, W.; Copos, C. A.; Lewis, O. L.; Guy, R. D. (2015): A poroelastic immersed boundary method with applications to cell biology. *Journal of Computational Physics*, vol. 282, no. Supplement C, pp. 77-97.

Taber, L.; Shi, Y.; Yang, L.; Bayly, P. (2011): A poroelastic model for cell crawling including mechanical coupling between cytoskeletal contraction and actin polymerization. *Journal of Mechanics of Materials and Structures*, vol. 6, no. 1-4, pp. 569-589.

Terzaghi, K. (1936): A fundamental fallacy in Earth pressure computations. *Boston Society Civil Engineers Journal*.

Thiriet, M. (2007): *Biology and Mechanics of Blood Flows: Part II: Mechanics and Medical Aspects*. Springer Science and Business Media.

Van Haastert, P. J. M. (2011): Amoeboid cells use protrusions for walking, gliding and swimming. *PLoS ONE*, vol. 6, no. 11.

Vuong, A. T.; Rauch, A. D.; Wall, W. A. (2017): A biochemo-mechano coupled, computational model combining membrane transport and pericellular proteolysis in tissue mechanics. *Proceedings of the Royal Society A: Mathematical, Physical and Engineering Science*, vol. 473, no. 2199.

Wei, F.; Lan, F.; Liu, B.; Liu, L.; Li, G. (2016): Poroelasticity of cell nuclei revealed through atomic force microscopy characterization. *Applied Physics Letters*, vol. 109, no. 21.

Wolf, K.; Mazo, I.; Leung, H.; Engelke, K.; von Andrian, U. H. et al. (2003): Com-pensation mechanism in tumor cell migration. *Journal of Cell Biology*, vol. 160, no. 2, pp. 267-277.

Woolley, T. E.; Gaffney, E. A.; Goriely, A. (2017): Random blebbing motion: A simple model linking cell structural properties to migration characteristics. *Physical Review E*, vol. 96, no. 1.

Yip, A. K.; Chiam, K. H.; Matsudaira, P. (2015): Traction stress analysis and modeling reveal that amoeboid migration in confined spaces is accompanied by expansive forces and requires the structural integrity of the membrane-cortex interactions. *Integrative Biology: Quantitative Biosciences from Nano to Macro*.

Zhou, E. H.; Martinez, F. D.; Fredberg, J. J. (2013): Cell rheology. *Nature Materials*, vol. 12, no. 3.

Zienkiewicz, O. C. (1999): *Computational Geomechanics with Special Reference to Earthquake Engineering*. Wiley, Chichester, New York.